

Stochastic Joint Alignment of Multiple Point Clouds for Profiled Blades 3-D Reconstruction

Weixing Peng, Yaonan Wang, Hui Zhang, *Member, IEEE*, Qing Zhu,
Zhiqiang Miao, *Member, IEEE*, and Mingtao Feng

Abstract—Joint registration of point clouds obtained from multiple views is a key step of reconstruction for blades. However, due to the structural and surface characteristics of blades, some views do not meet the overlap constraints of registration, which results in significant initial errors of pose estimation. Thus, we propose a novel approach to recover the accuracy of poses estimation. The proposed method is robust to overlap extent of views through a stochastic framework. The approach formulates a variable-parameters graph optimization problem. Then a simulated annealing algorithm is used to solve the global optimal parameters. The candidate parameters in the simulated annealing process are obtained through the improved UKF(unscattered Kalman filter), which reduces the initial errors and enhances the information matrices. The acceptance of the candidate parameters is determined by the optimization problem constrained by joint point correspondences and closed-loop consistency. And the parameters that can improve the registration accuracy are selected. We test our algorithm with simulated synthetic data and real data obtained by the robot measurement system. We compare the proposed algorithm with several state-of-the-art algorithms. The experimental results show that in the presence of significant initial errors, our method can estimate the poses more accurately and obtain better blade reconstructions.

Index Terms—Profiled Blades Reconstruction, point clouds registration, joint alignment, stochastic, consistency constraint.

I. INTRODUCTION

THE aero engine is the heart of an aircraft. The 3-D (three-dimensional) measurement is important to blade processing and quality monitoring. In order to meet the increasingly

Manuscript received August 24, 2020; revised October 21, 2020; accepted January 21, 2020. This work was supported in part by the National Key R&D Program of China (2018YFB1308200, 2020YFB1712600), in part by the National Natural Science Foundation of China under Grants 61733004, 62027810, 61903135, 61971071, 62076091, in part by the Postgraduate Scientific Research Innovation Project of Hunan Province (CX20200397), in part by the Science Technology Project of Hunan Province under Grant 2017XK2102, 2018GK2022, in part by the Natural Science Foundation of Hunan Province under Grant 2020JJ5090, and in part by the Independent Research Subject Funding from Hunan University State Key Laboratory of Advanced Design and Manufacturing for Vehicle Body. (Corresponding author: Qing Zhu.)

Weixing Peng, Yaonan Wang, Hui Zhang, Qing Zhu, Zhiqiang Miao, and Mingtao Feng are with the College of Electrical and Information Engineering, Hunan University, Changsha 410082, China, and also with the National Engineering Laboratory for Robot Visual Perception and Control, Changsha, China (e-mail:weixing peng@hnu.edu.cn; yaonan@hnu.edu.cn; zhanghuihb@126.com; zhuqing@hnu.edu.cn; miaoziqiang@hnu.edu.cn; mintfeng@hnu.edu.cn).

complex measurement requirements, it is urgent to develop 3-D measurement robots to realize automatic measurement. An autonomous measurement system aims to reconstruct the 3-D model of the blade and measure the dimension autonomously. The implementation of the system involves several steps, such as viewpoint planning, sensor positioning, 3D reconstruction, and surface matching that aligns measured points to a design model. A key problem that essentially arises in 3D reconstruction is the registration of point sets. The registration of two point sets, called pair-wise registration, attracts plenty of attention. Intuitively, multiple view registration can be converted into serials repeated pair-wise registrations, views registered against either neighboring view sequentially or a cumulative partial model [1] [2]. The common drawback of the repeated pair-wise registration strategy is that a cycle of relative motions between neighboring views would not be a closed loop, namely inconsistency. Thus, many methods tried to maintain the consistency to improve multiple views registration.

The first category performed registration for each view separately. Among the initial attempts, conducted by [3] and [4], a reference coordinate frame was selected in the topography of a view network, which minimized the total number of transformations from all other views to the selected one. Then the relative motions between the selected scan and others were repeatedly calculated one at a time, considering the shared and updated correspondences. [5] also incrementally registered views against a growing model based on point-to-plane correspondences. Benjemaa and Schmitt [6] proposed a nonlinear solution using the unit quaternions to accelerate the speed of the algorithm. The another method in [7], a multi-z-buffer algorithm, also aimed to accelerate algorithm by speeding the correspondences computation. The bias, yielded by only one set as reference, was avoided by randomizing the sequence of updates of individual scan motions. [8] pointed out that an intermediate view network with a newly integrated point set should be dealt with to be consistent for further reducing the accumulated error, and introduced a method alternated between handling wrong correspondences and registration based on signed point-to-surface distance field. [9] also proposed to alternate between computing a mean shape for all sets and registering the a scan against the mean shape.

The another category simultaneously considered all views. [10] minimized the distance between matches of all views. [11] and [12] employed the potential energy function of spring-

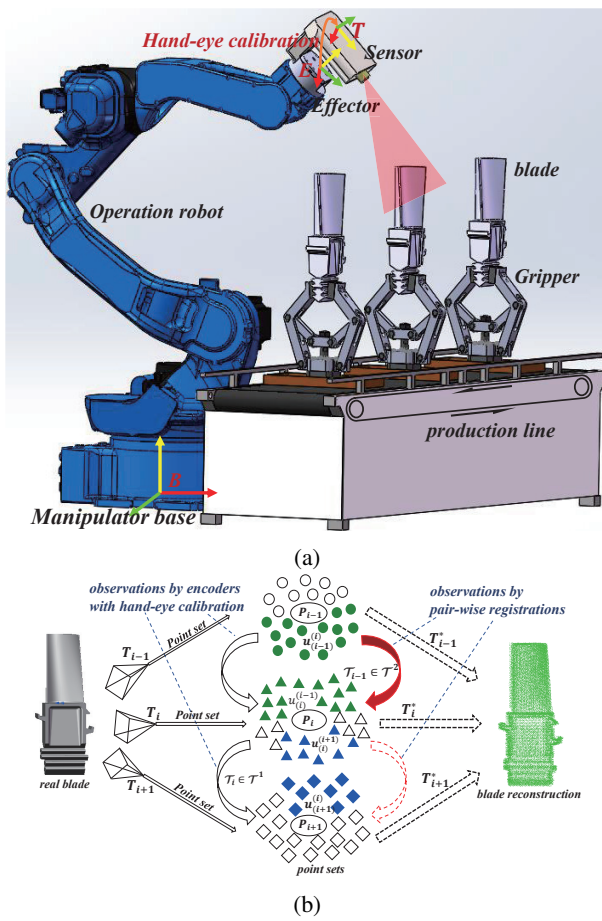


Fig. 1: (a) The robotic reconstruction system; (b) illustration of blade reconstruction

loaded dynamic systems as the objective function, respectively. [13] formulated a view-to-reference metric to measure the differences between the given and calculated pairwise registration transformation matrices, and determined the minima using Newton's method on manifold. These methods did not take the consistency into consideration, while [14] [15] only balanced the loop-closure over the view network without correspondence metric, which did not mean optimal view estimation though. [16] directly took the consistency as the constraint of the optimization formulated using total correspondence distance of all views, and derived an iterative solution by Lie algebra. However, these methods consider all matches fixed, which should be updated after the optimization of transformations. [17] performed exhaustive pairwise registrations followed by incorrect matches removal and determination of global surface consistency using a minimum spanning tree algorithm. [18] developed a strategy that alternated pairwise registration and Lie-algebraic motion average, simultaneously considering accurate correspondences determination and global consistency. [19] replaced the ICP method using trimmed-ICP method to compute pairwise motions.

There also existed many methods that would not specially balance the accumulated error. For instance, probabilistic methods have been developed. [20] represented the Mahalanobis distance between the estimates and measurements

as a constrained least-squares formulation. [21] [22] modeled each point set as a GMM (Gaussian Mixed Model) and a probabilistic mean shape was obtained by a convex combination of the parameterized models of sets. [23] suggested that these methods vitally relied on modeling of each cluster and requiring well structured points without outliers. [24] alternately reconstructed the mean shape and registered the views on it, with the strict assumption of given correspondences. Unlike [24], [23] and [25] aimed to simultaneously reconstruct the model of the object as a GMM model and a hybrid mixture model without known correspondences, respectively. In this way, the bias was avoided implicitly.

When it comes to the blades, registration of scans of multiple views becomes a more challenging task. On the one hand, aero engine blades are frequently designed as thin-walled and twisted space curved structures, which results in the overlaps between some scans and the target being insufficient. Requirements of pair-wise registration based on the ICP (iterative closest point) would not be met. On the other hand, the surface of the blades are deliberately smoothed to reduce the air resistance as much as possible. Thus, it is difficult to implement pair-wise registration based on matching features. As a consequence, the relative motions obtained merely through the pair-wise registration cannot constitute a complete optimization problem. We define it as an insufficient-overlap joint alignment problem.

Our work mainly makes three **contributions**. Firstly, we propose a stochastic joint alignment strategy. The strategy is based on graph optimization. For the transformations without sufficient overlaps, observations are obtained by encoders of manipulator cooperating with hand-eye calibration, which are not sensitive to overlaps. Besides, we use the simulated annealing algorithm to find the global optimal parameters for graph optimization. Thus, impact of large deviations and high uncertainties would be eliminated.

Secondly, we introduce an improved unscented Kalman filter between the transformation set and iterated one. The purpose is to determine candidate parameters with smaller observation errors and uncertainties.

Thirdly, a constrained joint registration optimization problem is formulated, and the iterative solution based on ADMMs (Alternating Direction Method of Multipliers) is derived. The optimization problem simultaneously considers the correspondences of all views, which are updated after each iteration. Further, the optimization selects initialization which yields a better minima through the simulated annealing architecture.

II. PROBLEM FORMULATION

First of all, we elaborate on the previously mentioned so-called insufficient-overlap joint registration problem on the robotic reconstruction platform. The meanings and interrelationships of the physical quantities involved in the mathematical model of the problem are explained in detail. The reconstruction system is illustrated in Fig. 1. A scanner sensor is mounted on the end-effector of the manipulator to gather 3-D point clouds from different views. Coordinate frames $\{T\}$, $\{B\}$ and $\{E\}$ are attached to bodies of the sensor,

manipulator base and end-effector, respectively. The relative pose between the frame $\{T\}$ and $\{E\}$ is calculated by hand-eye calibration. $T = \{T_i\}_{i=1}^I$ is also regarded as a pose set, where $T_i \in SE(3)$, $1 \leq i \leq I$ represents the pose of i th view. I is the total number of the views and $SE(3)$ means the special Euclidean group. With the T_1 fixed, denoted by W , T_i is a rigid transformation relative to W and expressed by a 4×4 homogeneous transformation matrix $\begin{bmatrix} \mathbf{R}_i & \mathbf{t}_i \\ \mathbf{0} & 1 \end{bmatrix}$. $\mathbf{R}_i \in SO(3)$ is a 3×3 rotation matrix and \mathbf{t}_i is a 3×1 translation vector. $SO(3)$ represents the special orthogonal group. A relative motion between two adjacent transformations, denoted by \mathcal{T}_i , is defined as $\mathcal{T}_i = T_i^{-1}T_{i+1}$. $\mathcal{T} = \{\mathcal{T}_i\}_{i=1}^I$ is the relative motion set. Here, \mathcal{T}_i is taken modulo I , so that if $i = I$, we refer to $\mathcal{T}_I = T_I^{-1}T_1$. The objective is to estimate the transformation T . In the iterations mentioned later, the superscript (s) or the subscript (s) represents the time s .

The $T_i \in T$ is provided with two kinds of observations, pair-wise registration results and manipulator odometry. The pair-wise registration result, denoted by $\phi_i \in SE(3)$, is obtained by ICP algorithm. The uncertainty of ϕ_i is represented by a covariance matrix Σ_i . The manipulator odometry, denoted by φ_i , is the relative pose between T_i and T_1 expressed in B , which are both calculated by compounding end-effector poses and the hand-eye calibration. The uncertainty of φ_i is represented by a covariance matrix Ψ_i . Notice that if the overlap of i th scan is insufficient, T_i is unobserved by the pair-wise registration. But T_i , for $1 \leq i \leq I$, can always be observed by manipulator odometry.

Denote the observations for all $\mathcal{T}_i \in \mathcal{T}$ as a set $\chi = \{\chi_i\}_{i=1}^I$, $\chi_i \in SE(3)$. And the uncertainties of all $\chi_i \in \chi$ are represented by a covariance matrix set $\Gamma = \{\Gamma_i\}_{i=1}^I$. The χ is split into two subsets χ^1 and χ^2 , namely $\chi = \chi^1 \cup \chi^2$. $\chi^1 = \{\chi_k^1\}_{k=1}^K$ is the set of relative motion observations, which are compounded through transformation observations obtained by the manipulator odometry. $\chi^2 = \{\chi_l^2\}_{l=1}^L$ is the set of relative motion observations, which compounded through transformation observations obtained by registrations. Only when both of the transformations T_i and T_{i+1} can be observed by the pair-wise registrations, the observation of relative motion \mathcal{T}_i is calculated in the way of χ_i^2 . Similarly, Γ is divided into two subsets $\Gamma^1 = \{\Gamma_k^1\}_{k=1}^K$ and $\Gamma^2 = \{\Gamma_l^2\}_{l=1}^L$. Accordingly, \mathcal{T} is divided into two subsets $\mathcal{T}^1 = \{\mathcal{T}_k^1\}_{k=1}^K$ and $\mathcal{T}^2 = \{\mathcal{T}_l^2\}_{l=1}^L$.

Let P_i be the point set of i th scan. For P_i , $u_{(i)}^{(i+1)} = \{u_{(i)1}^{(i+1)} \dots u_{(i)n}^{(i+1)} \dots u_{(i)N_i}^{(i+1)}\} \in P_i$ represents the corresponding point set to the neighboring point set P_{i+1} , which is determined by a correspondence determination algorithm. Similarly, the corresponding point set of P_{i+1} to P_i is represented by $u_{(i+1)}^{(i)} = \{u_{(i+1)1}^{(i)} \dots u_{(i+1)n}^{(i)} \dots u_{(i+1)N_i}^{(i)}\} \in P_{i+1}$, where $1 \leq n \leq N_i$ is the index of the corresponding points. With the coordinate frame \mathcal{W} of P_1 fixed, T_i maps P_i to the frame \mathcal{W} , such that all points sets form a point cloud model in the frame \mathcal{W} .

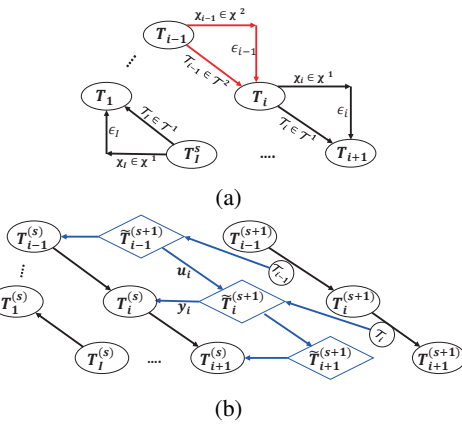


Fig. 2: (a) Graph of pose estimation; (b) dynamic Bayesian network

A. Uncertainties on Lie Groups

Since the subsequent graph optimization and unscented Kalman filter theories both involve the concept of uncertainties on the Lie group, we recall the definitions and basic properties of the Lie group, Lie algebra and random variables on Lie groups. With the observation ϕ_i , T_i is considered as a random variables on Lie groups, and the Gaussian probability distribution $T_i \sim \mathcal{N}(\phi_i, \Sigma_i)$ is defined as

$$T_i = \phi_i \exp(\sigma_i), \sigma_i \sim \mathcal{N}(0, \Sigma_i), \quad (1)$$

where $\exp(\cdot)$ is the exponential map and \mathcal{N} is the Gaussian distribution in Euclidean space. As for \mathcal{T}_i , whose observation $\chi_i \in \chi^2$, the Gaussian probability distribution $\mathcal{T}_i \sim \mathcal{N}(\chi_i, \Gamma_i)$ is defined as

$$\mathcal{T}_i = \chi_i \exp(\gamma_i), \gamma_i \sim \mathcal{N}(0, \Gamma_i), \quad (2)$$

where $\chi_i = \phi_i^- \phi_{i+1}$ and $\Gamma_i = \Gamma_{i4th} \approx \Sigma_i + \Sigma'_{i+1} + \frac{1}{12}(\mathcal{A}_1 \Sigma'_{i+1} + \Sigma'_{i+1} \mathcal{A}_1^\top + \mathcal{A}'_2 \Sigma_i + \Sigma_i \mathcal{A}'_2^\top)$ according to equation (55) in [26].

While the T_i is observed by φ_i , a random sample of T_i is drawn from

$$T_i = \varphi_i \exp(\psi_i), \psi_i \sim \mathcal{N}(0, \Psi_i), \quad (3)$$

In terms of \mathcal{T}_i , whose observation $\chi_i \in \chi^1$, the Gaussian probability distribution $\mathcal{T}_i \sim \mathcal{N}(\chi_i, \Gamma_i)$ is defined as equation (2), with the mean $\chi_i = \varphi_i^- \varphi_{i+1}$ and covariance $\Gamma_i = \Gamma_{i4th} \approx \Psi_i + \Psi'_{i+1} + \frac{1}{12}(\mathcal{A}_1 \Psi'_{i+1} + \Psi'_{i+1} \mathcal{A}_1^\top + \mathcal{A}'_2 \Psi_i + \Psi_i \mathcal{A}'_2^\top)$.

B. Graph Optimization for Transformation Estimation

With the observation of relative motion \mathcal{T}_i and initialization of each pose known, a graph optimization method is introduced to determine the optimal poses of the scanner sensor. Hence, a graph is construed, as illustrated in Fig. 2(a). Each node is attached to a transformation T_i . And an edge connecting two nodes is labeled with a relative motion \mathcal{T}_i . The

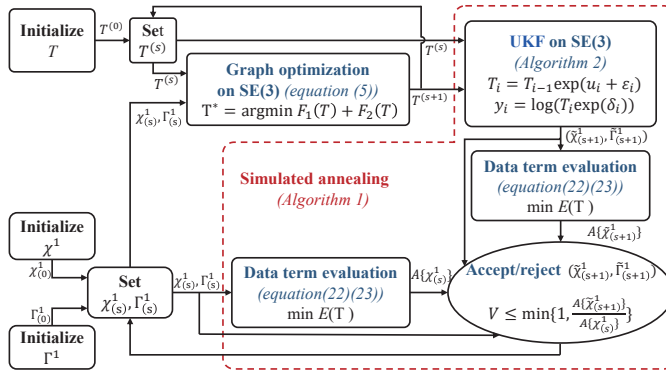


Fig. 3: Architecture of the proposed framework.

transformation estimation is an optimization problem, which is formulated as

$$\begin{aligned} T^* &= \underset{T}{\operatorname{argmin}} \frac{1}{2} \sum_{i=1}^I \epsilon_i^\top \Gamma_i^{-1} \epsilon_i \\ &= \underset{T}{\operatorname{argmin}} \frac{1}{2} \sum_{i=1}^I \log(\chi_i^{-1} \mathcal{T}_i)^\top \Gamma_i^{-1} \log(\chi_i^{-1} \mathcal{T}_i) \end{aligned} \quad (4)$$

where ϵ_i is the error term between \mathcal{T}_i , and its observation χ_i and the $\log(\cdot)$ is the Lie logarithm map.

C. Deficiency Caused by Insufficient-overlap Observation

Although the graph optimization method can calm the pose errors to a certain extent, the following analysis is given to discuss the influences of the initial errors and the observations with greater uncertainties. There are two observations of relative motions, thus, problem (4) can be rewritten as

$$\begin{aligned} T^* &= \underset{T}{\operatorname{argmin}} F_1(T) + F_2(T) \\ &= \underset{T}{\operatorname{argmin}} \frac{1}{2} \sum_{k=1}^K \log(\chi_k^{-1} \mathcal{T}_k^1)^\top \Gamma_k^{1-} (\chi_k^{-1} \mathcal{T}_k^1) \\ &\quad + \frac{1}{2} \sum_{l=1}^L \log(\chi_l^{-1} \mathcal{T}_l^2)^\top \Gamma_l^{2-} (\chi_l^{-1} \mathcal{T}_l^2) \end{aligned} \quad (5)$$

Optimization (5) is non-convex, and can be solved by a iterative solution on manifold [27]. Notice that the observation errors and uncertainties of the manipulator odometry are much larger than that of pair-wise registrations, which will cause two problems: (1) The errors of initial guesses of transformations, which compose \mathcal{T}_k^1 , is much larger; (2) The corresponding information matrices are smaller. As a consequence, the optimization process is more inclined to adjust the transformations observed by manipulator odometry significantly, and the accumulated error of transformations observed by registrations will be reduced slightly.

III. PROPOSED METHOD

To attack the problem caused by insufficient overlaps, we propose a variable-parameter graph optimization method, whose framework is illustrated in Fig. 3. The adjustment of these parameters is based on the framework of the simulated

annealing algorithm. The two main elements of simulated annealing have been redesigned, namely the candidate parameter generator and the acceptance function. The candidate parameter generator is implemented using the unscented Kalman filter on the Lie group, whose system input and observation parameters are calculated from the graph. The acceptance function considers pairs of matching points of all adjacent views to form an optimization term. It aims to obtain a set of poses that minimize the sum of distances between all matching points, that is, an accurate result obtained from rough initialization through optimization. In general, before each iteration of optimization for problem (5), the parameters $\chi_k^1 \in \chi^1$ and $\Gamma_k^1 \in \Gamma^1$ will try to be adjusted in order to improve the estimation accuracy of the transformations.

A. Simulated Annealing for Parameters of Graph

Parameters χ_k^1 and Γ_k^1 of problem (5) are adjustable, thus, optimization can be further rewritten as:

$$(T^*, \chi^{1*}, \Gamma^{1*}) = \underset{T, \chi^1, \Gamma^1}{\operatorname{argmin}} F_1(T, \chi^1, \Gamma^1) + F_2(T). \quad (6)$$

Problem (6) is non-convex, a similar strategy as alternating direction method is adopted to solve it. With χ_k^1 and Γ_k^1 fixed, variables $T_i \in T$, which compose \mathcal{T}_i , iterated as described in literature [27]. As for the parameters χ_k^1 and Γ_k^1 , we use simulated annealing algorithm to adjust them to find the global minima of problem (6).

Simulated annealing algorithm is a sampling based method for the global optimization problem. The extended continuous version was presented in [28], and we resort it, which is described in Algorithm 1. With the framework of parameters adjustment, the generator function $G(h_{(s)})$ and acceptance function $\Phi\{\chi_{(s)}^1, \tilde{\chi}_{(s+1)}^1\}$ needed to be designed.

B. UKF on SE(3) for Candidate Parameters

We employ an unscented Kalman filter as the generator function, that is, the mean $\kappa = \{\kappa_i\}_i^I$ and covariance $P = \{P_i\}_i^I$ of the transform T are estimated by the filter, and then are compounded into new observations of relative motions $\tilde{\chi}^1$ and $\tilde{\Gamma}^1$. As shown in Fig. 2(b), the transformation without optimization iteration is denoted as T^s , and the transformation iterated is denoted as $T^{(s+1)}$. A dynamic Bayesian network between $T^{(s)}$ and $T^{(s+1)}$ is built, where $T^{(s)}$ is regarded as measurement, and $T^{(s+1)}$ is used to calculate the system input. Considering $T \in SE(3)$, we design an unscented Kalman filter based on [29], and the state space model is:

$$T_i = T_{i-1} \exp(u_i + \varepsilon_i) \quad (7)$$

$$y_i = \log(T_i \exp(\delta_i)), \quad (8)$$

where the $u_i \in se(3)$ is the system input, $\varepsilon_i \in se(3)$ is the state transition noise, $y_i \in se(3)$ is the measurement and δ_i is the measurement noise, respectively. Compared with the general Lie group version of the unscented Kalman filter in [29], our filter is dedicated to updating the parameters of the graph structure, so we have special definitions for the above variables. The u_i is defined using a relative motion, we have

$$u_i = \log(\chi_i^{(s+1)}), \quad \varepsilon_i \sim \mathcal{N}(0, \Gamma_i^{(s+1)}) \quad (9)$$

Algorithm 1: Continuous Simulated Annealing

- 1 Initialize variables:
 $(\chi_{(0)}^1, \Gamma_{(0)}^1), h_{(0)} = \{(\chi_{(0)}^1, \Gamma_{(0)}^1)\}, s = 0, t_{(0)} = 1;$
- 2 Generate candidate variables:
 $(\tilde{\chi}_{(s+1)}^1, \tilde{\Gamma}_{(s+1)}^1) \sim G(h_{(s)});$
- 3 Decide candidate variable accepted or rejected:
 sample a uniform value \mathcal{V} in $[0, 1]$
 $(\chi_{(s+1)}^1, \Gamma_{(s+1)}^1) = \begin{cases} (\tilde{\chi}_{(s+1)}^1, \tilde{\Gamma}_{(s+1)}^1), \mathcal{V} \leq \Phi\{\chi_{(s)}^1, \tilde{\chi}_{(s+1)}^1\} \\ (\chi_{(s)}^1, \Gamma_{(s)}^1) \quad , otherwise \end{cases};$
- 4 Update variable set:
 $h_{(s+1)} = h_{(s)} \cup \{(\chi_{(s+1)}^1, \Gamma_{(s+1)}^1)\};$
- 5 Cool the temperature: $t_{(s+1)} = U(h_{(s+1)});$
- 6 Quit if stop criteria reached or $s = s + 1$ and go back to Step2;

If measurement y_i is a matrix, it leads to a nontrivial approximation of posterior $p(T_i|y_i)$ and a complex covariance [29]. Thus, the measurement is mapped into a vector space, and measurement is defined as

$$y_i = \log(\kappa_i^{(s)}), \quad \delta_i \sim \mathcal{N}(0, P_i^{(s)}) \quad (10)$$

Without loss of generality, the filter is divided into two steps: control update and measurement update.

1) *Control update:* The control update calculates the propagated state mean $\bar{\kappa}$ and covariance \bar{P} . Compared with [29], the control update process of our filter adopts a high-order linear approximation method with a smaller error, instead of a random linearized unscented transformation through a weighted statistical linear regression. According to pose compounding method proposed in [26], the propagated state mean $\bar{\kappa}_i$ and covariance \bar{P}_i of T_i are determined as

$$\bar{\kappa}_i = \kappa_{i-1} \exp(u_i) \quad (11)$$

$$\bar{P}_i = P_{i4th} \approx$$

$$P_i + P_{i+1}' + \frac{1}{12}(\mathcal{A}_1 P_{i+1}' + P_{i+1} \mathcal{A}_1^\top + \mathcal{A}_2' P_i + P_i \mathcal{A}_2'^\top). \quad (12)$$

2) *Measurement update:* The goal of measurement update is to calculate the posterior probability $p(T_i|y_i)$. With the y_i , δ_i , $\bar{\kappa}_i$ and \bar{P}_i available, an unscented transform is used to obtain $p(T_i|y_i) \sim (\kappa_i, P_i)$. First, a quantity $\sigma \sim (0, \bar{P}_i)$ is introduced, followed by sampling a set of sigma points $\beta_m^t = [\sigma_m^\top, \delta_m^\top]$, with $m = 0, \dots, 24$, from the matrix $P^{aug} = diag\{\bar{\kappa}_i, \bar{P}_i\}$, as

$$U\Sigma V^t = SVD((l + \lambda)P^{aug})$$

$$\beta_m^t = \begin{cases} \mathbf{0} & m = 0 \\ col(U)_m & 1 \leq m \leq 12 \\ -col(U)_{m-12} & 13 \leq m \leq 24 \end{cases}, \quad (13)$$

where the *SVD* (Singular Value Decomposition) is adopted to prevent the P^{aug} from illness, instead of directly using $\sqrt{(1 + \lambda)P^{aug}}$ in [29]. It will fall into an ill-conditioned state

Algorithm 2: Unscented Kalman Filter on SE(3)

- Input:** $\kappa_{i-1}, P_{i-1}, u_i, \varepsilon_i, y_i, \delta_i, \alpha$;
- Output:** κ_i, P_i
- 1 $\bar{\kappa}_i = \kappa_{i-1} \exp(u_i);$
- 2 $\bar{P}_i = P_{i4th};$
- 3 $\lambda = (\alpha^2 - 1) * 12;$
- 4 $W_s^0 = \frac{\lambda}{\lambda+l}, W_c^0 = \frac{\lambda}{\lambda+l} + (3 - \alpha^2),$
 $W_s^m = W_c^m = \frac{1/2}{\lambda+l}, m = 1, \dots, 24;$
- 5 $P^{aug} = diag(\bar{\kappa}_i, \bar{P}_i);$
- 6 $U\Sigma V^t = SVD((l + \lambda)P^{aug});$
- 7 $\beta_0 = \mathbf{0}, m = 0; \beta_m = col(U)_m, m = 0, \dots, 12;$
 $\beta_m = -col(U)_m, m = 13, \dots, 24;$
- 8 $[\sigma_m^\top, \delta_m^\top] = \beta_m^t, m = 1, \dots, 24;$
- 9 $y_i^m = ln(\bar{\kappa}_i \exp(\sigma_m) \exp(\delta_m));$
- 10 $\bar{y} = \sum_{m=0}^{24} W_s^m y_m;$
- 11 $P_{y_i y_i} = \sum_{m=0}^{24} W_c^m (y_i^m - \bar{y})(y_i^m - \bar{y})^\top;$
- 12 $P_{\beta y_i} = \sum_{m=0}^{24} W_c^m \alpha_i (y_i^m - \bar{y})^\top;$
- 13 $\begin{bmatrix} \bar{\xi} \\ * \end{bmatrix} = P_{\beta Y_i} P_{y_i Y_i}^{-1} (y_i - \bar{y});$
- 14 $\kappa_i = \bar{\kappa}_i \exp(\bar{\xi});$
- 15 $P_i = \bar{\Sigma}_i - P_{\beta y_i} (P_{\beta y_i} P_{y_i Y_i}^{-1})^\top;$

when negative elements appear in the matrix P^{aug} . Then β_m^\top is passed through measurement equation, as

$$y_i^m = ln(\bar{\kappa}_i \exp(\sigma_m) \exp(\delta_m)). \quad (14)$$

Then the measurement mean \bar{y}_i , the measurement covariance $P_{y_i y_i}$, and the cross-covariance $P_{\beta y_i}$ are calculated. Thus, the determination of posterior probability $p(T_i|y_i)$ is transformed into an approximation of posterior probability $p(\xi|y_i) \sim \mathcal{N}(\bar{\xi}|P_i)$. In the end, the mean κ_i can be obtained. Concretely, the whole unscented Kalman filer on $SE(3)$ is summarized in Algorithm 2. With the $\bar{\kappa}$ and \bar{P} estimated, the observations by manipulator odometry are replaced by them to calculate the observation of \mathcal{T}^1 as aforementioned.

C. Constrained Data Term Evaluation

The candidate parameters of optimization (6) are $(\tilde{\chi}_{(s+1)}^1, \tilde{\Gamma}_{(s+1)}^1)$, which are accepted or rejected as the new parameters relying on the acceptance function $\Phi\{(\chi_{(s)}^1, \Gamma_{(s)}^1), (\tilde{\chi}_{(s+1)}^1, \tilde{\Gamma}_{(s+1)}^1)\}$. Traditionally, the acceptance function is designed to judge if the objective function declined. However, the minima of objective function does not mean the optimal estimation of T , because the data is ignored in the formulation. Thus, a novel acceptance function is designed, which takes three factors into account instead.

1) *Data term:* with the correspondence points between two scans known, the accuracy of relative motion \mathcal{T}_i is evaluated by the distance \mathcal{D}_i . Conceivably, a data term to evaluate a

group of relative motion \mathcal{T} can be defined using a union of \mathcal{D}_i , expressed by

$$\mathcal{D}(T) = \sum_{i=1}^I \mathcal{D}_i = \sum_{i=1}^I \sum_{n=1}^{N_i} \left\| \mathcal{T}_i u_{(i)n}^{(i+1)} - u_{(i+1)n}^{(i)} \right\|_F^2 \quad (15)$$

where $\|\cdot\|_F$ is F-norm of a matrix, \mathcal{T}_i is rewritten as a 3×4 transformation $[\mathbf{R}_i \ \mathbf{t}_i]$, $u_{(i)n}^{(i+1)}$ is a homogeneous coordinate $(x, y, z, 1)$ and $u_{(i+1)n}^{(i)}$ is a coordinate (x, y, z) . Motivated by [30], define some matrices as

$$U_i^{i+1} = [u_{(1)}^{(2)} \dots u_{(n)}^{(n+1)} \dots u_{(N_i)}^{(1)}], \quad (16)$$

$$U_{i+1}^i = [u_{(2)}^{(1)} \dots u_{(n+1)}^{(n)} \dots u_{(1)}^{(N_i)}], \quad (17)$$

where U_i^{i+1} is of size $4 \times N_i$, and U_{i+1}^i is of size $3 \times N_i$. Then, equation(23) can be rewritten as

$$\mathcal{D}(T) = \sum_{i=1}^I \left\| \mathcal{T}_i U_i^{i+1} - U_{i+1}^i \right\|_F^2 \quad (18)$$

2) *Consistency constraint*: ideally, a set of transformations arranged in a cycle, as illustrated in Fig. 2(a), should compose to a identity matrix $I_4 \in \mathbb{R}^{4 \times 4}$, which is expressed as

$$\prod_{i=1}^I \begin{bmatrix} \mathbf{R}_i & \mathbf{t}_i \\ \mathbf{0} & 1 \end{bmatrix} = I_4. \quad (19)$$

However, \mathcal{T}_i in equation (18) is 3×4 transformation. Thus, the rotation \mathbf{R}_i and translation \mathbf{t}_i are decoupled, so that equation (19) is rewritten as

$$\prod_{i=1}^I \mathbf{R}_i = I_3. \quad (20)$$

$$\mathbf{R}_1 \mathbf{R}_2 \dots \mathbf{R}_{I-1} \mathbf{t}_I + \dots + \mathbf{R}_1 \mathbf{R}_2 \dots \mathbf{R}_{i-1} \mathbf{t}_i + \dots + \mathbf{t}_1 = \mathbf{0}$$

3) *Orthogonality constraint*: $\mathcal{T}_i \in SE(3)$, thus, the rotation R_i is orthogonal,

$$\mathbf{R}_i^\top \mathbf{R}_i = I_3 \text{ and } |\mathbf{R}_i| = 1, \forall i \in [1 \dots I]. \quad (21)$$

In summary, these terms yield a constrained optimization problem:

$$\begin{aligned} \min E(\mathcal{T}) = & \min \sum_{i=1}^I \left\| \mathcal{T}_i U_i^{i+1} - U_{i+1}^i \right\|_F^2 + \lambda \sum_{i=1}^I \left\| A \mathcal{T}_i - \mathbf{R}_i \right\|_F^2 \\ \text{s.t. } & \mathbf{R}_i^\top \mathbf{R}_i = I_3 \text{ and } |\mathbf{R}_i| = 1, \forall i \in [1 \dots I], \\ & \prod_{i=1}^I \mathcal{T}_i = I_3, \end{aligned} \quad (22)$$

where λ is a constant coefficient and $A = [\mathbf{I}_3 \ \mathbf{0}]_{3 \times 3}$ is a matrix used to extract rotation from \mathcal{T}_i . Once the optimal $\mathcal{T}_i^* = [\mathbf{R}_i^* \ \mathbf{t}_i^*]$ of equation(22) is obtained, the optimal translation \mathbf{t}_i^* are easily computed with

$$\mathbf{t}_i^* = \min \sum_{i=1}^I \left\| \mathbf{t}_i - \mathbf{t}_i^* \right\|^2 \quad (23)$$

$$\mathbf{R}_1^* \mathbf{R}_2^* \dots \mathbf{R}_{I-1}^* \mathbf{t}_I + \dots + \mathbf{R}_1^* \mathbf{R}_2^* \dots \mathbf{R}_{i-1}^* \mathbf{t}_i + \dots + \mathbf{t}_1 = \mathbf{0}$$

Optimization (22) is non-convex due to the constraint. In order to obtain a treatable optimization, Lagrange multiplier method is employed and the augmented Lagrangian function is

$$\begin{aligned} \mathcal{L}(\mathcal{T}, Y, \mu) = & \sum_{i=1}^I \left\| \mathcal{T}_i U_i^{i+1} - U_{i+1}^i \right\|_F^2 + \left\langle Y, I_3 - \prod_{i=1}^I \mathbf{R}_i \right\rangle \\ & + \frac{\mu}{2} \left\| Y, I_3 - \prod_{i=1}^I \mathbf{R}_i \right\|_F^2 + \lambda \sum_{i=1}^I \left\| A \mathcal{T}_i - \mathbf{R}_i \right\|_F^2 \\ \text{s.t. } & \mathbf{R}_i^\top \mathbf{R}_i = I_3 \text{ and } |\mathbf{R}_i| = 1, \forall i \in [1 \dots I], \end{aligned} \quad (24)$$

where Y is the Lagrangian multiplier, μ is a penalty parameter, and $\langle \cdot, \cdot \rangle$ denotes inner product of two matrices. Optimization(24) is still non-convex, for which we use the ADMMs to solve. Hence, the \mathcal{T} , Y and μ at each iteration are obtained using

$$\left\{ \begin{aligned} \mathcal{T}_i^{(k+1)} = & \underset{\mathcal{T}_i}{\operatorname{argmin}} \left\| \mathcal{T}_i U_i^{i+1(k)} - U_{i+1}^{i(k)} \right\|_F^2 \\ & + \left\| A \mathcal{T}_i - \mathbf{R}_i^{(k)} \right\|_F^2, \\ \mathbf{R}_i^{(k+1)} = & \underset{\mathbf{R}_i}{\operatorname{argmin}} \lambda \left\| A \mathcal{T}_i^{(k)} - \mathbf{R}_i \right\|_F^2 \\ & + \left\langle Y^{(k)}, I_3 - \mathbf{R}_1^{(k)} \dots \mathbf{R}_i \dots \mathbf{R}_I^{(k)} \right\rangle \\ & + \frac{\mu}{2} \left\| Y^{(k)}, I_3 - \mathbf{R}_1^{(k)} \dots \mathbf{R}_i \dots \mathbf{R}_I^{(k)} \right\|_F^2 \\ \text{s.t. } & \mathbf{R}_i^\top \mathbf{R}_i = I_3 \text{ and } |\mathbf{R}_i| = 1, \\ Y^{(k+1)} = & Y^{(k)} + \mu^{(k)} \left(I_3 - \prod_{i=1}^I \mathbf{R}_i^{(k)} \right), \\ \mu^{(k+1)} = & \rho \mu^{(k)}, \rho > 1 \end{aligned} \right. \quad (25)$$

Thus, we define the acceptance function as

$$\Phi\{\chi_{(s)}^1, \tilde{\chi}_{(s+1)}^1\} = \min\{1, \frac{\mathcal{A}\{\tilde{\chi}_{(s+1)}^1\}}{\mathcal{A}\{\chi_{(s)}^1\}}\}, \quad (26)$$

where $\mathcal{A}\{\tilde{\chi}_{(s+1)}^1\} = \min E(\mathcal{T})$, while iterating using $\mathcal{T}^0 = \tilde{\chi}_{(s+1)}^1$; and $\mathcal{A}\{\chi_{(s)}^1\} = \min E(\mathcal{T})$, while iterating using $\mathcal{T}^0 = \chi_{(s)}^1$. Combining the optimization(6) and optimization (22)-(23) through the simulated annealing method, both of them obtain global minima.

It is worth to mention that the fine registration of the constrained data term optimization is used as the final pose estimation. Therefore, the proposed algorithm can also be understood as loops of looking for a better initialization and constrained data term registration refinement. The influences of insufficient overlaps on the pose estimation are gradually eliminated during the loops.

IV. EXPERIMENTS

We implement some tests on synthetic data sets and a real data set obtained from our robotic measurement system. The performances of five methods, namely the proposed stochastic joint alignment method, the sequential ICP method, the graph optimization method [27], the error distribution method [14], and exception-maximization joint alignment method [23], are

TABLE I: AVERAGE DEVIATIONS BETWEEN ACTUAL TRANSFORMATIONS AND TRUE VALUES

Method	blade1				blade2				blade3			
	sufficient overlap		insufficient overlap		sufficient overlap		insufficient overlap		sufficient overlap		insufficient overlap	
	translation	rotation	translation	rotation	translation	rotation	translation	rotation	translation	rotation	translation	rotation
SICP	1.882	0.053	17.321	0.332	2.102	0.041	17.321	0.332	2.071	0.042	17.321	0.332
GO	1.227	0.034	8.642	0.220	1.666	0.029	9.602	0.219	1.165	0.028	10.176	0.243
ED	4.875	0.143	6.263	0.176	5.266	0.121	6.726	0.164	5.116	0.135	6.534	0.157
JRMPC	0.418	0.014	1.726	0.066	0.605	0.019	1.585	0.081	0.370	0.011	1.642	0.079
SJA	0.523	0.017	0.936	0.038	0.416	0.014	1.052	0.042	0.327	0.013	0.831	0.036

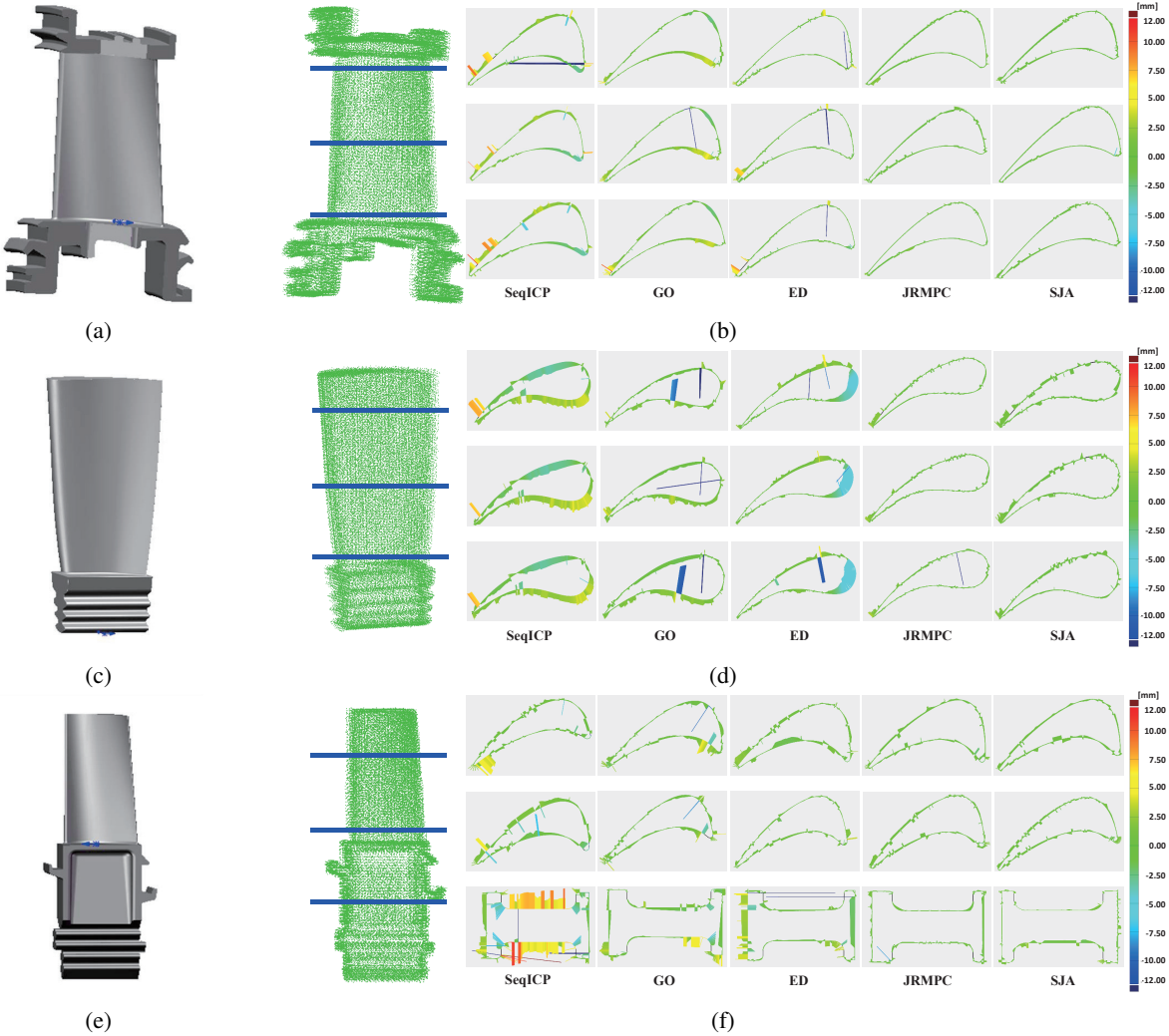


Fig. 4: (a)(c)(e) are synthetic blade models; (b)(d)(f) are reconstructions by our method and chromatograms of cross section by all methods.

compared together. For convenience, the five methods are abbreviated as SJA, SICP, GO, ED, and JRMPC method. The graph optimization method was implemented using the g2o (general graph optimization) framework, and JRMPC was carried out through the codes kindly shared by the authors.

A. Synthetic Data Tests

As illustrated in Fig. 4(a)(c)(e), three blade models are adopted to synthesize data sets. The synthetic data sets are obtained through simulated 3-D range sensor on the platform of gazebo in ROS, which contains 10 point sets from different

views and available true values of view poses. The sequential pair-wise registration strategy through ICP algorithm is performed to provide for observation \mathcal{T}^2 . Then initial errors are artificially added to all view poses to simulate observation \mathcal{T}^1 . Subsequently, the five methods are employed to calculate the transformation T . We use 100 iterations for the SJA, GO and JRMPC method. Specially, the data term evaluation is given another 40 iterations for the optimization problem (22) and (23). In order to highlight the effectiveness of our method on the pose estimation of scans with insufficient overlaps, indicators were divided into two parts to evaluate, namely the

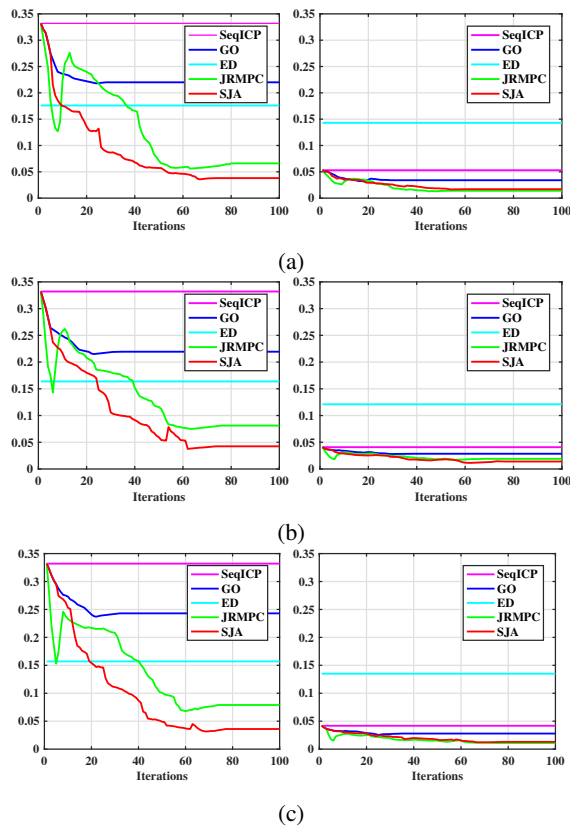


Fig. 5: (a)(b)(c) are iterations of the rotation errors for corresponding blades in proper order (right and left for insufficient and sufficient part, respectively)

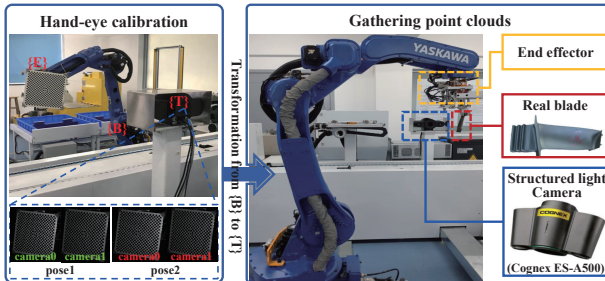


Fig. 6: Real reconstruction system.

scans with sufficient overlap and insufficient overlap.

Fig. 5(a)(b)(c) show square of the F-norm of absolute deviation between the actual rotation matrix and the true value, averaged over the numbers of related poses, for the 100 iterations of the methods. Although the SICP and ED have closed-form results, constants of their results are plotted for comparison. Our method converges when the optimization (22) reaches the global minimum. Because pure graph optimization always converges, and when optimization (22) reaches the global minimum, the parameters of graph optimization (6) no longer change. The part of the rapid decline is due to the fact that the parameters generated by the filter are accepted. Remarkably, for the part with insufficient scan overlap, GO converges with a significantly large error and the JRMPC has

a slight larger error than SJA method. Thus, it reveals that adjusting the parameters of the graph by the proposed SJA method can effectively improve the convergence.

Table I records the error when converges. On the one hand, for the scans with enough overlap, the proposed SJA method and JRMPC method achieve the most considerable accuracy. The accuracy of The GO method and ED method is improved compared to the SICP method, but still inferior to the other two methods. Specifically, only the values of JRMPC are slightly lower than that of SJA in terms of average deviations of blade 1 and blade 3. The SICP method uses point cloud registration or robot odometry to calculate relative motion between the two adjacent views one by one. Then the pose of each view is calculated by compounding all relative motions between itself and the view pose selected as the reference. Even poses with sufficient overlap are affected by the accumulated error, not to mention the large errors caused by the robot odometry and hand-eye calibration. GO initializes the nodes and edges of the graph based on the results of SICP, and optimizes the pose nodes by minimizing the sum of the errors between edges and the observations. However, as analyzed in section II.C, when the overlap is insufficient, the information matrix of an ICP registration observation is much larger than that of a robot odometry observation. Thus, the pose observed by the ICP can only be optimized in a small range to maintain a smaller error in the objective function. Therefore, the improvement of SICP by GO is small. An error averaging technology adopted by ED will share the larger pose errors observed by the robot odometry to the poses observed by ICP registrations. Therefore, the errors of the poses obtained by ED will increase, compared with that of SICP. The proposed SJA continuously adjusts the parameters of the graph to reduce the effects of excessive initial guess errors and small information matrices caused by insufficient overlaps. And matching points of all adjacent views are considered jointly to achieve fine registration, which can effectively improve the defects of SICP. JRMPC regards all the points as a sample of a Gaussian mixture model, turning the problem of multi-view registration into a clustering problem. This approach treats all the point sets on an equal footing [23], thus there exists no offsets and accumulated errors. Due to the selection of experimental parameters, the average offset of the proposed SJA is slightly larger than that of JRMPC for blade1 and blade3, but it is smaller for blade 2. In general, both JRMPC and SJA have achieved good results while the overlaps are enough. On the other hand, for the scans with insufficient overlaps, our method can significantly reduce the errors compared to other methods. The Go method cannot effectively restore the accuracies of poses with insufficient scan overlaps due to the large initial displacements and small information matrices. In terms of JRMPC, the accuracy would be relatively sensitive to the extent of overlaps under the influence of initializations [23]. As for the proposed SJA method, the initializations of optimization for data term were updated to obtain a better minima, which yields robustness to the extend of overlaps.

Fig. 4(b)(d)(f) show the reconstructed models and cross-section chromatograms on the reconstructions, which reflect the errors between measuring points and the design model. On

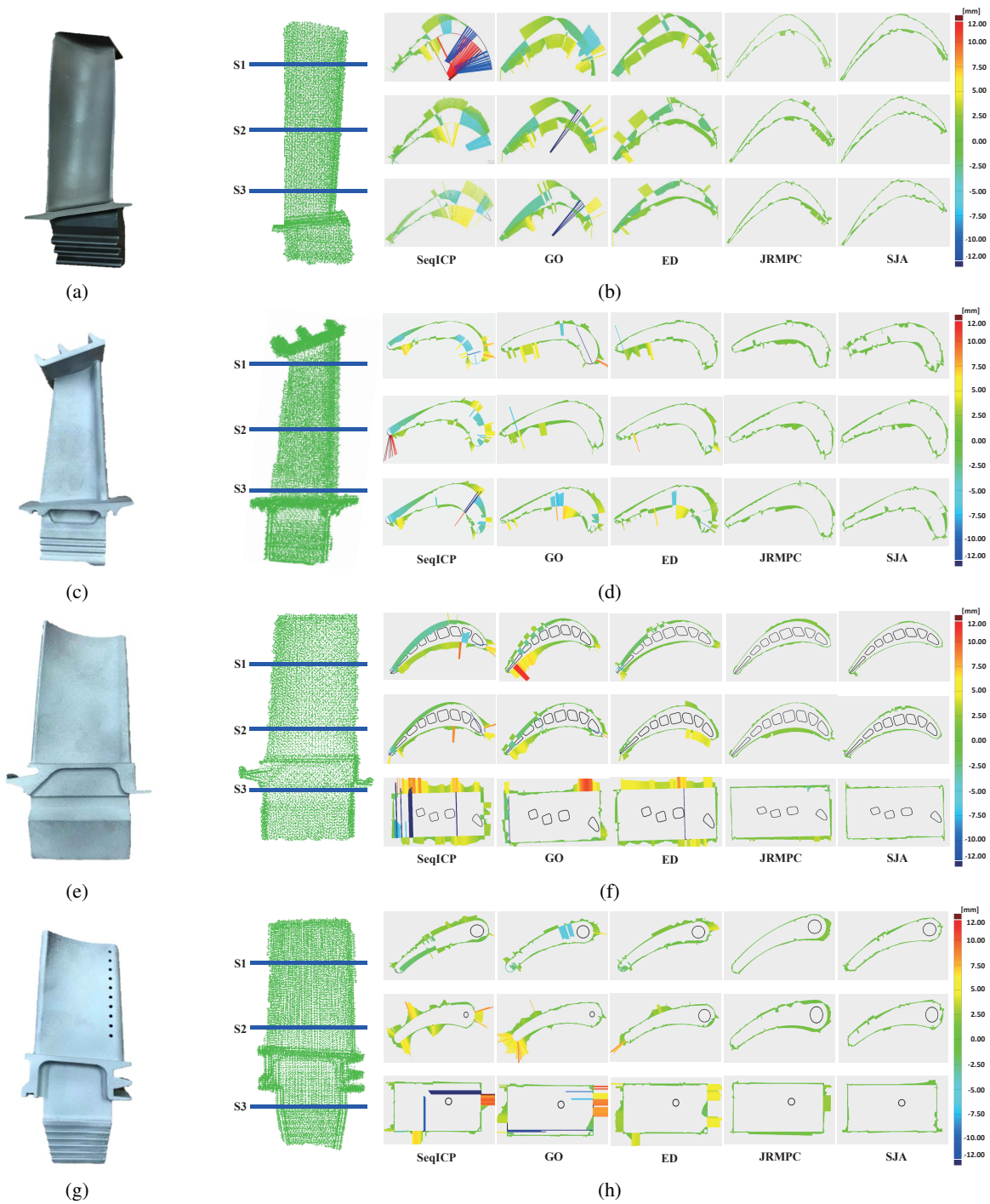


Fig. 7: (a)(c)(e)(g) are real blades, and named blade1, blade2, blade3 and blade4, respectively; (b)(d)(f)(h) are reconstructions by our method and chromatograms of cross section by all methods.

the whole, in the chromatographic analysis of the three blades, our method can obtain the smallest color difference and peak error. However, it is worth to mention that the JMRPC method is as good as our method in the performance of chromatic aberration on certain cross sections, which is reflected in all the three reconstructed models. It shows that performance of the proposed SJA and JMRPC is the best, under the condition of sufficient overlaps. While the overlaps are insufficient, SJA can effectively reduce the reconstruction errors.

B. Real Data Tests

The real point sets are gathered through the robotic measurement system, shown in Fig. 6, which mainly consists of a Yaskawa DX200 manipulator and a Cognex ES-A5000 binocular structure light camera. The camera is stably fixed on a platform. And the blade is grasped by the manipulator, whose pose relative to the camera is changed to gather point cloud from different views.

For each blade, the real data contains 10 point sets, which

TABLE II: THE MEAN DISTANCE AND DISTANCE STANDARD DEVIATION OF THE MEASURING POINTS ON THE SECTIONS OBTAINED BY DIFFERENT METHODS

blade	cross-section	SICP		GO		ED		JMRPC		SJA	
		mean (mm)	std deviation (mm)								
blade1	s1	1.62	6.21	0.35	2.52	0.73	1.51	0.05	0.39	0.04	0.31
	s2	0.94	3.83	0.18	2.68	0.37	1.43	0.19	0.47	-0.01	0.29
	s3	-0.06	4.61	0.14	2.74	0.17	1.32	0.09	0.45	0.03	0.25
blade2	s1	-0.20	1.95	0.33	1.59	0.23	1.01	0.05	0.44	-0.05	0.34
	s2	-0.09	2.06	-0.02	2.48	-0.08	1.72	0.03	0.45	0.02	0.28
	s3	-0.40	1.96	-0.12	2.21	0.15	1.47	0.02	0.42	0.01	0.25
blade3	s1	-0.31	3.31	0.97	2.38	-0.07	1.35	0.34	0.59	0.04	0.28
	s2	-0.49	3.06	0.16	1.87	0.62	1.35	0.42	0.67	0.06	0.23
	s3	2.11	5.14	0.55	2.26	1.93	1.77	0.26	1.07	0.09	0.24
blade4	s1	-0.15	1.86	-0.26	1.56	0.05	1.38	0.15	0.45	0.07	0.19
	s2	1.06	1.58	0.80	1.48	0.18	0.90	0.14	0.53	0.07	0.27
	s3	0.25	2.75	0.46	2.29	0.53	1.54	0.35	0.55	0.06	0.20

are down sampled before reconstruction. With the coordinate frame of the first scan fixed, the initial guesses of other poses and two groups of relative motions are calculated by SICP and encoders cooperating with hand-eye calibration, respectively. The true values of the camera poses are difficult to know, which prevents us from discussing the effectiveness of the algorithm using the pose errors. Therefore, only the comparisons between the reconstructed models and the design template models can be used to evaluate these algorithms, although there are inherent errors between a design template and the actual blade. Four kinds of real blades with different structural characteristics are employed to test the feasibility of the proposed method, as illustrated in Fig.7 (a)(c)(e)(g).

Fig. 7 (b)(d)(f)(h) show the integrated models of the blades reconstructed using all views and cross-section chromatograms yielded by inserting three section planes. For the four blades, many areas of the cross sections relative to the SICP method are shown in dark red and blue. Part of the cross sections relative to GO and ED methods are also shown dark red and blue. In terms of JMRPC method, only a slight yellow color appears on the third sections of blade3 and blade4. However, basically all areas are showed in green on the sections of the proposed SJA method. Thus, As a baseline and initial configuration, the reconstruction errors of SICP are the largest due to accumulated errors and insufficient overlaps. Obviously, GO and ED perform more poorly in eliminating reconstruction errors than SJA and EMJA, which is shown in all the chromatograms of the three cross sections. In a small number of chromatographic indicators, JMRPC even showed a slight accuracy advantage over SJA. But in most of the situations, SJA has smaller errors and neater cross-section outlines.

Considering the mismatches between measuring points and real points, Table II presents the mean distance and distance std (standard deviation) of the measuring points on the sections. The JMRPC and proposed SJA method obtain significantly smaller mean distance and distance std than the other methods. Moreover, compared with JMRPC, the proposed SJA has shown advantages on most sections. In consequence, the proposed strategy is more robust to the initial configuration

and the extent of overlaps.

V. CONCLUSION

In this paper, a pose estimation problem caused by insufficient overlaps has been proposed. To solve this problem, a stochastic joint registration framework based on simulated annealing has been developed to adjust the parameters of the graph optimization. The framework has used unscented Kalman filter on SE(3) to find candidate parameters, and innovatively constructed a constrained simultaneous correspondences optimization term to evaluate the benefice of parameters to the joint registration accuracy. Experiments have proved that insufficient overlaps will indeed cause large errors in the pose estimation of the views. The employed unscented Kalman filter could reduce the errors and uncertainties of the observations. On the whole, the proposed method could not only maintain estimation accuracy with overlaps sufficient, but also restore the estimation accuracy from a rough initialization better than other methods do, while lacing of overlap extent. The proposed method has showed good robustness to overlap extent and initial displacements.

REFERENCES

- [1] R. Bergevin and M. Soucy, "Towards a general multi-view registration technique," *IEEE Transactions on Pattern Analysis and Machine Intelligence*, vol. 18, no. 5, pp. P.540–547, 1996.
- [2] U. Castellani, A. Fusiello, and V. Murino, "Registration of multiple acoustic range views for underwater scene reconstruction," *Computer Vision and Image Understanding*, vol. 87, no. 1-3, pp. 78–89, 2002.
- [3] Gagnon, Soucy, Bergevin, and Laurendeau, "Registration of multiple range views for automatic 3-d model building," in *1994 Proceedings of IEEE Conference on Computer Vision and Pattern Recognition*, pp. 581–586, 1994.
- [4] R. Bergevin, M. Soucy, H. Gagnon, and D. Laurendeau, "Towards a general multi-view registration technique," *IEEE Transactions on Pattern Analysis and Machine Intelligence*, vol. 18, no. 5, pp. 540–547, 1996.
- [5] Y. Chen and G. Medioni, "Object modeling by registration of multiple range images," *Image and Vision Computing*, vol. 10, no. 3, pp. 145–155, 1992.
- [6] R. Benjema, e. H. Schmitt, Francis", and B. Neumann, "A solution for the registration of multiple 3d point sets using unit quaternions," in *Proc. Eur. Conf.Comput. Vis.*, pp. 34–50, 1998.
- [7] R. Benjema and F. Schmitt, "Fast global registration of 3d sampled surfaces using a multi-z-buffer technique," in *Proceedings. International Conference on Recent Advances in 3-D Digital Imaging and Modeling (Cat. No.97TB100134)*, pp. 113–120, 1997.

- [8] T. Masuda, "Registration and integration of multiple range images by matching signed distance fields for object shape modeling," *Computer Vision and Image Understanding*, vol. 87, DOI <https://doi.org/10.1006/cviu.2002.0982>, no. 1, pp. 51 – 65, 2002.
- [9] X. Pennec, "Enhanced, robust genetic algorithms for multiview range image registration," in *Multiple Registration and Mean Rigid Shapes?Application to the 3D Case*, pp. 178–185, 1996.
- [10] J. Williams and M. Bennamoun, "Simultaneous registration of multiple corresponding point sets," *Computer Vision and Image Understanding*, vol. 81, no. 1, pp. 117–142, 2001.
- [11] D. W. Eggert, A. W. Fitzgibbon, and R. B. Fisher, "Simultaneous registration of multiple range views for use in reverse engineering of cad models," *Computer Vision and Image Understanding*, vol. 69, no. 3, pp. 253–272, 1998.
- [12] P. J. Neugebauer, "Geometrical cloning of 3d objects via simultaneous registration of multiple range images," in *Proceedings of 1997 International Conference on Shape Modeling and Applications*, pp. 130–139, 1997.
- [13] S. Krishnan, P. Y. Lee, J. B. Moore, and S. Venkatasubramanian, "Global registration of multiple 3d point sets via optimization-on-a-manifold," presented at the *Eurographics Symp. Geometry Processing*, 2005.
- [14] G. C. Sharp, S. W. Lee, and D. K. Wehe, "Multiview registration of 3d scenes by minimizing error between coordinate frames," *IEEE Transactions on Pattern Analysis and Machine Intelligence*, vol. 26, no. 8, pp. 1037–1050, 2004.
- [15] V. M. Govindu, "Lie-algebraic averaging for globally consistent motion estimation," in *Proceedings of the 2004 IEEE Computer Society Conference on Computer Vision and Pattern Recognition, 2004. CVPR 2004.*, vol. 1, pp. I–I, 2004.
- [16] S. Shih, Y. Chuang, and T. Yu, "An efficient and accurate method for the relaxation of multiview registration error," *IEEE Transactions on Image Processing*, vol. 17, no. 6, pp. 968–981, 2008.
- [17] T. Oishi, A. Nakazawa, R. Sagawa, and R. Kurazume, "Parallel alignment of a large number of range images," in *Fourth International Conference on 3-D Digital Imaging and Modeling, 2003. 3DIM 2003. Proceedings.*, pp. 195–202, 2003.
- [18] V. M. Govindu and A. Pooja, "On averaging multiview relations for 3d scan registration," *IEEE Transactions on Image Processing*, vol. 23, no. 3, pp. 1289–1302, 2014.
- [19] Z. Li, J. Zhu, K. Lan, C. Li, and C. Fang, "Improved techniques for multi-view registration with motion averaging," in *2014 2nd International Conference on 3D Vision*, vol. 1, pp. 713–719, 2014.
- [20] J. A. Williams, M. Bennamoun, and S. Latham, "Multiple view 3d registration: a review and a new technique," in *IEEE SMC'99 Conference Proceedings. 1999 IEEE International Conference on Systems, Man, and Cybernetics (Cat. No.99CH37028)*, vol. 3, pp. 497–502 vol.3, 1999.
- [21] B. Jian and B. C. Vemuri, "Robust point set registration using gaussian mixture models," *IEEE Transactions on Pattern Analysis and Machine Intelligence*, vol. 33, no. 8, pp. 1633–1645, 2011.
- [22] F. Wang, B. C. Vemuri, A. Rangarajan, and S. J. Eisenschenk, "Simultaneous nonrigid registration of multiple point sets and atlas construction," *IEEE Transactions on Pattern Analysis and Machine Intelligence*, vol. 30, no. 11, pp. 2011–2022, 2008.
- [23] G. D. Evangelidis and R. Horaud, "Joint alignment of multiple point sets with batch and incremental expectation-maximization," *IEEE Transactions on Pattern Analysis and Machine Intelligence*, vol. 40, no. 6, pp. 1397–1410, 2018.
- [24] J. Goldberger, "Registration of multiple point sets using the em algorithm," in *Proceedings of the Seventh IEEE International Conference on Computer Vision*, vol. 2, pp. 730–736 vol.2, 1999.
- [25] Z. Min, J. Wang, and M. Q. Meng, "Joint rigid registration of multiple generalized point sets with hybrid mixture models," *IEEE Transactions on Automation Science and Engineering*, vol. 17, no. 1, pp. 334–347, 2020.
- [26] T. D. Barfoot and P. T. Furgale, "Associating uncertainty with three-dimensional poses for use in estimation problems," *IEEE Transactions on Robotics*, vol. 30, no. 3, pp. 679–693, 2014.
- [27] G. Grisetti, R. Kummerle, C. Stachniss, and W. Burgard, "A tutorial on graph-based slam," *IEEE Intelligent Transportation Systems Magazine*, vol. 2, no. 4, pp. 31–43, 2010.
- [28] I. Kolesov, J. Lee, G. Sharp, P. Vela, and A. Tannenbaum, "A stochastic approach to diffeomorphic point set registration with landmark constraints," *IEEE Transactions on Pattern Analysis and Machine Intelligence*, vol. 38, no. 2, pp. 238–251, 2016.
- [29] M. Brossard, S. Bonnabel, and J. Condomines, "Unscented kalman filtering on lie groups," in *2017 IEEE/RSJ International Conference on Intelligent Robots and Systems (IROS)*, pp. 2485–2491, 2017.
- [30] J. Yang, D. Guo, K. Li, Z. Wu, and Y. Lai, "Global 3d non-rigid registration of deformable objects using a single rgb-d camera," *IEEE Transactions on Image Processing*, vol. 28, no. 10, pp. 4746–4761, 2019.



Weixing Peng received the B.S. degrees in automation science from the College of Information Science and Technology, Donghua University, Shanghai, China, in 2016. He is currently pursuing the Ph.D. degree in control theory and control engineering in Hunan University. His current research interests include vision servo control, viewpoint planning and 3D reconstruction of autonomous measurement robot technology for engine blade.



Yaonan Wang received the Ph.D. degree in electrical engineering from Hunan University, Changsha, China, in 1994. From 1998 to 2000, he was a Senior Humboldt Fellow in Germany, and, from 2001 to 2004, he was a Visiting Professor with the University of Bremen, Bremen, Germany. Since 1995, he has been a Professor with the College of Electrical and Information Engineering, Hunan University. His current research interests include robotics and image processing.



Hui Zhang received the B.S., M.S., and Ph.D. degrees in pattern recognition and intelligent system from Hunan University, Changsha, China, in 2004, 2007, and 2012, respectively. He is currently a Professor with the College of Robot, Hunan University, Changsha, China. Hunan University. His research interests include machine vision, deep learning, defect detection.



Qing Zhu received the B.S., M.S., and Ph.D. degrees in electrical engineering from Hunan University, Changsha, China, in 1989, 2000, and 2008, respectively. She is currently an Associate Professor and a Ph.D. Supervisor with the College of Electrical and Information Engineering, Hunan University. Her current research interests include image processing and communication technology.



Zhiqiang Miao received the B.S. and Ph.D. degrees in Electrical and Information Engineering from Hunan University, Changsha, China, in 2010 and 2016, respectively. From 2014 to 2015, he was a Visiting Scholar with the University of New Mexico, Albuquerque, NM, USA. He is currently an Associate Professor with the College of Electrical and Information Engineering, Hunan University. His current research interests include multirobot systems, visual servoing, and nonlinear control.



Mingtao Feng received the Ph.D. degree at the College of Electrical and Information Engineering, Hunan University, in 2019. He was a visiting PhD student at the School of Computer Science and Software Engineering, The University of Western Australia from 2016 to 2018. He is currently a lecturer with the the School of Computer Science and Technology at Xidian University. His research interests include image processing, computer vision and machine learning.